

Efficient Training of Generalizable Visuomotor Policies via Control-Aware Augmentation

Yinuo Zhao^{1,*}, Kun Wu^{2,*}, Tianjiao Yi¹, Zhiyuan Xu², Xiaozhu Ju², Zhengping Che²
Chi Harold Liu¹, Jian Tang²

Abstract

Improving generalization is one key challenge in embodied AI, where obtaining large-scale datasets across diverse scenarios is costly. Traditional weak augmentations, such as cropping and flipping, are insufficient for improving a model’s performance in new environments. Existing data augmentation methods often disrupt task-relevant information in images, potentially degrading performance. To overcome these challenges, we introduce **EAGLE**—an **Efficient trAining framework for GeneraLizable visuomotor policies**—that improves upon existing methods by: 1) enhancing generalization by applying augmentation only to control-related regions identified through a self-supervised control-aware mask; and 2) improving training stability and efficiency by distilling knowledge from an expert to a visuomotor student policy, which is then deployed to unseen environments without further fine-tuning. Comprehensive experiments on three domains—including the DMControl Generalization Benchmark, the enhanced Robot Manipulation Distraction Benchmark, and a long-sequential drawer-opening task—validate the effectiveness of our method. Project website: <https://vrl-eagle.github.io/>

1. Introduction

End-to-end visuomotor policies learn low-level controls directly from high-dimensional inputs using either reinforcement learning or imitation learning algorithms. These learning paradigms yield promising results in embodied AI tasks such as robot manipulation [4, 24], autonomous navigation [1], and locomotion [49, 52]. However, visuomotor policies heavily rely on visual inputs for decision-making and control, making them susceptible to performance degradation when faced with changes in background, distractors, or viewpoints. This deficiency cannot be mitigated through

reinforcement nor imitation learning alone.

One promising technique to reduce the impact of these visual discrepancies is Data Augmentation (DA) [11, 17, 41, 49, 50]. *Weak augmentations*, like random cropping, rotation, and flipping, consistently enhance generalization, but with modest improvements. In contrast, *strong augmentations* such as *random conv* [29] and *random overlay* [16], boosting generalization capabilities through significantly diversifying the data. Followed by this, algorithms [5, 11, 17] propose to maintain consistency in visual features or control values between augmented and original observations. Nevertheless, *strong augmentations* can indiscriminately distort the entire observation space, disrupting the control-related environmental structures and dynamics captured in the data. This often complicates training and destabilizes both learning and testing phases. While previous research has focused on augmenting specific areas within the observational space, these methods typically depend on dense reward functions [2, 12] and are limited to identifying dynamic objects [47] without considering their task relevance. Recently, vision foundation models like SAM [26] have shown strong generalization abilities. However, they still require fine-tuning or human-given priors to identify task-relevant regions in the observation space. Therefore, automatically identifying control-related pixels for generalizable visuomotor policies still remains challenging, especially in tasks with long horizons and non-informative rewards.

To enhance generalization and maintain stability, in this paper, we propose an **Efficient trAining** framework for **GeneraLizable** visuomotor policies (EAGLE) that can identify control-related information and facilitate zero-shot deployment in unseen environments. Instead of learning a generalizable visuomotor policy directly, we adopt a distillation approach for efficient and stable training. Specifically, EAGLE consists of two jointly optimized modules: 1) A control-aware augmentation module that adaptively learns to highlight control-related pixels using spatial-temporal data from the following distillation module, employing a self-supervised reconstruction task; 2) A privilege-guided distillation module to extract control

¹Beijing Institute of Technology, {ynzhao, tjyi}@bit.edu.cn, liuchi02@gmail.com

²Beijing Innovation Center of Humanoid Robotics, {gongda.wu, eric.xu, jason.ju, z.che, jian.tang}@x-humanoid.com

*These authors contributed equally.

knowledge from an expert agent trained with a standard deep reinforcement learning (DRL) algorithm. The DRL expert receives low-level environment states. It is worth noting that this privileged information is readily obtainable [3, 13, 28, 36, 40] in a robotic simulated environment, and would only be accessed during training.

To evaluate the zero-shot generalization abilities, we conducted experiments over three domains, including the commonly used DMControl Generalization Benchmark [16], an enhanced Robot Manipulation Distraction Benchmark based on [21] with visual changes on the control-irrelevant background and distractors, a self-built challenging drawer-operation generalization platform based on NVIDIA Isaac Sim [34]. Extensive experimental results show that our method advances the state-of-the-art in terms of generalization ability and computation cost.

We summarize our contributions as follows:

- We propose an efficient training framework for generalizable visuomotor policies to achieve zero-shot generalization to unseen environments with visual changes.
- We introduce a method to derive a control-aware mask within a self-supervised reconstruction structure, eliminating the need for additional labels or reward signals.
- To enhance training stability and efficiency, we develop a strategy to learn visuomotor policies by distilling knowledge from a privileged expert pre-trained on low-level environmental states.
- Extensive comparative and ablation studies across three benchmarks well validate the effectiveness of our method.

2. Related works

Generalization performance degradation results from data distribution shifts from the training environments to testing ones. Common distribution shifts include changes in visual appearance [2, 11, 30, 53], object distractors [32, 47], environmental structures [6, 31], and viewpoints [48]. In this work, we primarily focus on visual changes but also experiment with distractors and viewpoint variations.

Improving the generalization of visuomotor policies remains a significant challenge [6, 7, 22, 33, 35, 37, 38, 46, 51, 56]. Regularization techniques like dropout [42], entropy regularization [14, 58], and batch normalization [19] are commonly used for generalization improvements in supervised learning. However, for more complex visuomotor policies, they offer limited improvements and may reduce sampling efficiency [6, 50].

Data augmentation (DA) is a simple yet efficient technique for enhancing the zero-shot generalization capabilities of visuomotor policies. *Weak augmentations*, such as geometric (e.g., random cropping) and photometric (e.g., grayscale conversion) transformations, are easily integrated with various policy learning algorithms but offer limited generalization benefits. In contrast, *strong augmenta-*

tions [2, 11, 53] introduce highly diverse samples, potentially bridging generalization gaps; however, they can lead to a diverged action distribution during training due to visual variability [53]. DA methods generally focus on consistency between the augmented and original inputs, either in visual features—such as in SGQN [2], SODA [16], and VAI [47]—or in output actions, as with SECANT [11], TLDA [53], and SVEA [17]. EAGLE improves visuomotor policies by aligning their outputs directly with the expert’s, falling in the latter category. The control-aware augmentation module in our method is similar to that in VAI [47], but focuses on identifying control-related regions rather than merely the dynamic foreground. This approach allows for the augmentation of whole control-irrelevant regions, leading to improved generalization. Besides DA, other approaches focus on auxiliary tasks or redesigning training objectives to learn invariant and robust representations, such as the information bottleneck [10], bisimulation metrics [25, 57], and pretrained backbones [54]. EAGLE is orthogonal to these techniques and can be combined for further improvements.

Policy distillation has been widely explored in various scenarios and tasks [3, 8, 28]. Similar to SECANT [11], our method uses distillation to maintain stability, while leveraging a privileged expert to reduce computational costs and enhance performance. Unlike SECANT [11], which relies on mix of augmentations, our approach shows that one well-chosen *strong augmentation* method is enough for improving generalization with a more efficient training process for robot learning. In other domains, LBC [3] trains a student policy with limited sensor input under the supervision of an expert with privileged information in the CARLA simulator [9] for autonomous driving tasks. Zhou *et al.* [60] have developed a task distillation framework to transfer navigation policies between different simulators. Similarly, ITER [20] transfers accumulated knowledge into newly initialized networks to mitigate non-stationary effects. The privileged expert, trained in simulators, is readily accessible. With the recent advances in vision foundation models [26, 39], obtaining state information such as object positions in real environments has become easier, enabling the deployment of privileged experts in actual platforms.

3. Method

In this section, we introduce an efficient training framework for generalizable visuomotor policies (EAGLE). The overall goal of EAGLE is to directly learn visuomotor policies that are invariant and capable of zero-shot generalization. As shown in Fig 1, EAGLE consists of two simultaneously optimized modules: a control-aware augmentation module (left) and a privilege-guided distillation module (right). The former module retrieves temporal data from the replay buffer and conducts a self-supervised reconstruction task,

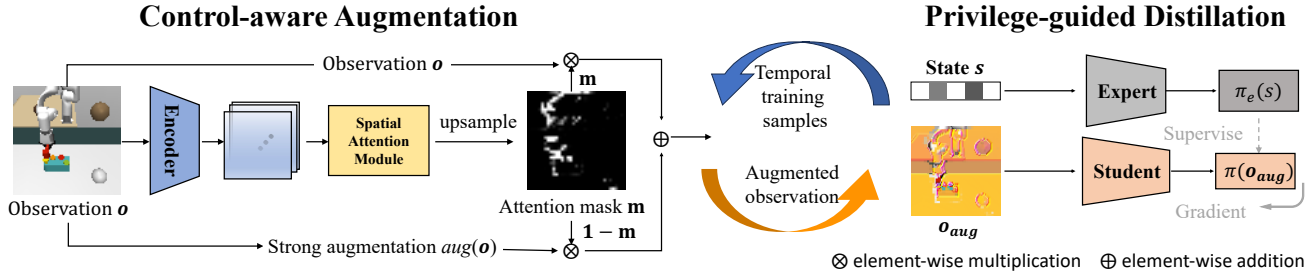


Figure 1. Overview of our method.

accompanied by three auxiliary losses, to identify control-related pixels. The latter module augments the observation input and distills knowledge from a pretrained DRL expert (which processes only environment states) into the visuomotor student network (which processes only image observations). After training is completed, the visuomotor policy can be reliably deployed in complex environments with visual variations, without the need for fine-tuning or additional supervision.

3.1. Control-aware Data Augmentation

The control-aware data augmentation module is designed to learn an attention mask that efficiently identifies control-related regions, distinguishing them from irrelevant areas such as static backgrounds and unrelated objects. In this way, we can confidently use *strong augmentation* without fear of compromising essential information for policy learning, thereby enhancing generalization ability. To achieve this, we develop a lightweight mask-generating model using Convolutional Block Attention [44] (CBA) and train a clear attention mask in a self-supervised manner.

As shown in Fig. 2, the control-aware data augmentation module consists of four networks: 1) An image encoder $f_e(\cdot)$ that takes the observation \mathbf{o} as input and outputs a feature map \mathbf{z} , 2) A spatial attention block $f_a(\cdot)$ that receives \mathbf{z} and outputs the attention mask \mathbf{m} , 3) A decoder $f_d(\cdot)$ that processes the feature maps to produce the reconstructed image $\hat{\mathbf{o}}$, 4) A control prediction module $f_{ctl}(\cdot)$ that utilizes control-related feature maps to generate the predicted control \hat{a} .

Below, we detail the methods for learning the control-aware mask that differentiates between control-related and control-irrelevant regions, introducing a self-supervised reconstruction task complemented by three auxiliary losses to facilitate efficient learning.

At the beginning, we randomly sample a source image \mathbf{o}_t from the replay buffer and obtain its next transition \mathbf{o}_{t+1} as the target image. We derive the feature map $\mathbf{z}_t = f_e(\mathbf{o}_t)$ and the attention mask $\mathbf{m}_t = f_a(\mathbf{z}_t)$ from the source image. Similarly, we obtain \mathbf{z}_{t+1} and \mathbf{m}_{t+1} from the target image. Thus, $\mathbf{z}_t \otimes \mathbf{m}_t$ and $\mathbf{z}_{t+1} \otimes \mathbf{m}_{t+1}$ specifically rep-

resent the control-related features extracted by the control-aware masks from the source and target images. Following the approach of [47], we synthesize the latent feature $\hat{\mathbf{z}}_{t+1}$ for reconstructing the target image using the equation:

$$\hat{\mathbf{z}}_{t+1} = \mathbf{z}_{t+1} \otimes \mathbf{m}_{t+1} + \mathbf{z}_t \otimes (1 - \mathbf{m}_t) \otimes (1 - \mathbf{m}_{t+1}), \quad (1)$$

where the operator \otimes denotes element-wise multiplication across channels. By multiplying the $1 - \mathbf{m}_{t+1}$ in the second term, we can reduce the interference from the intersection part of $1 - \mathbf{m}_t$ and \mathbf{m}_{t+1} , enhancing the accuracy of the latent feature for the target image. Finally, we synthesize the target image by processing $\hat{\mathbf{z}}_{t+1}$ through the decoder $f_d(\cdot)$. The reconstruction loss is calculated as follows:

$$\mathcal{L}_{rec}(\mathbf{o}_t, \mathbf{o}_{t+1}) = \|f_d(\hat{\mathbf{z}}_{t+1}) - \mathbf{o}_{t+1}\|_2^2. \quad (2)$$

Then, we introduce three auxiliary losses to facilitate learning a clear control-aware mask. First, we add an auto-encoder loss \mathcal{L}_{ae} by directly reconstructing from the target feature \mathbf{z}_{t+1} to capture more accurate latent information. The auto-encoder loss is computed as follows:

$$\mathcal{L}_{ae}(\mathbf{o}_{t+1}) = \|f_d(\mathbf{z}_{t+1}) - \mathbf{o}_{t+1}\|_2^2. \quad (3)$$

Second, to extract essential control-related regions, we construct a control prediction loss \mathcal{L}_{ctl} to predict the control from the control-related features of the source and target images:

$$\mathcal{L}_{ctl}(\mathbf{o}_t, \mathbf{o}_{t+1}) = \|f_{ctl}(\mathbf{z}_t \otimes \mathbf{m}_t, \mathbf{z}_{t+1} \otimes \mathbf{m}_{t+1}) - a_t\|_2^2, \quad (4)$$

where \mathbf{z}_t and \mathbf{m}_t are the feature map and the attention mask from the source image, respectively. To ensure stable training, the gradient to \mathbf{z}_t is detached, as shown in Fig. 2.

Lastly, we add a sparsity penalty loss \mathcal{L}_{sps} to flexibly control the generated attention mask. $\mathcal{L}_{sps} = \|\mathbf{m}_j\|_1$. The overall loss function is defined as:

$$\mathcal{L}_{att} = \mathcal{L}_{rec} + \mathcal{L}_{ae} + \beta \mathcal{L}_{ctl} + \lambda \mathcal{L}_{sps}, \quad (5)$$

where β and λ are hyper-parameters that balance the contribution of auxiliary losses relative to the reconstruction loss.

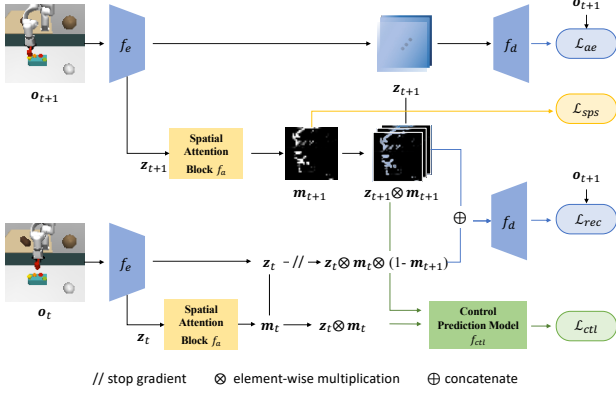


Figure 2. Control-aware data augmentation module.

The image encoder $f_e(\cdot)$, spatial attention block $f_a(\cdot)$, decoder $f_d(\cdot)$, and control prediction model f_{ctl} are optimized simultaneously. To stabilize training, we stop gradient propagation along the branch of the source image o_t , as illustrated in Fig 2. To apply observation-level control-aware attention masks m , we directly upsample them to the observation scale and only augment control-irrelevant regions. The augmented image o_{aug} is obtained as follows:

$$o_{aug} = o \otimes m + aug(o) \otimes (1 - m), \quad (6)$$

where $aug(\cdot)$ refers to *strong augmentation* operations like *random conv* [29] and *random overlay* [16]. This strategy allows the augmentation of control-irrelevant pixels while preserving control-related pixels for decision-making.

3.2. Privilege-guided Policy Distillation

While *strong augmentation* introduces diverse inductive biases to reduce the generalization gaps, it also complicates policy optimization significantly [11]. Specifically, the agent must learn to output the same action for two completely different augmented observations derived from the original observation. This requirement often leads to high variance in value function estimates, making the training process unstable for any standard RL algorithm. Therefore, instead of directly training visuomotor policies with DRL, we opt to distill knowledge from a privileged DRL agent to the student visuomotor policies.

The privilege expert π_e receives environmental states s as inputs. Note that using privileged control-related information is reasonable in training environments, typically controlled simulators where such information is readily available [3, 28]. For example, in LBC [3], privileged information like object positions, road features, and traffic signals is distilled into a sensorimotor agent for autonomous driving tasks. Moreover, with the rapid development of vision foundation models [26, 39], extracting state information such as object positions in real environments has be-

come more feasible, facilitating the use of privileged experts in actual applications.

The expert policy is trained in a standard RL paradigm and is compatible with any RL algorithm. In practice, we build our implementation on the top of DrQv2 [49] due to its broad adoption in continuous control tasks [15, 45, 55].

The distillation process employs the L-2 loss, defined as:

$$\hat{\mathcal{L}}(\pi_\theta) = \mathbb{E}_{(o,s) \sim \mathcal{D}} [\|\pi_\theta(o_{aug}) - \pi_e(s)\|_2^2]. \quad (7)$$

Following the method in SECANT [11], we alternately use π_e and π to collect environmental samples, storing them in a replay buffer \mathcal{D} . At each iteration, we simultaneously 1) update the context-aware data augmentation module using Eqn. (5), and 2) optimize the visuomotor policy according to Eqn. (7).

3.3. Theoretical Insights

In [18], the authors study the effect of data augmentation in the case of binary classification under Rademacher complexity. Here, we also provide theoretical Insights behind EAGLE under Rademacher complexity.

The visuomotor policy network is parameterized by θ and outputs a k -dimensional continuous action $\pi_\theta(o) \in \mathbb{R}^k$. We aim to compute the Rademacher complexity of the policy function class: $\mathcal{F} = \{\pi_\theta \mid \theta \in \Theta\}$. For each dimension j , the empirical Rademacher complexity is given by:

$$\hat{\mathfrak{R}}_N(\mathcal{F}_j) = \frac{1}{N} \mathbb{E}_\sigma \left[\sup_{\theta \in \Theta} \sum_{i=1}^N \sigma_i \pi_{\theta,j}(o_i) \right]. \quad (8)$$

where $\pi_{\theta,j}(o_i)$ is the output of the policy network at sample o_i in dimension j , σ_i are independent Rademacher random variables taking values $+1$ or -1 with equal probability, N is the number of i.i.d. data samples.

Then, the total empirical Rademacher complexity for the function class \mathcal{F} is the sum over all dimensions:

$$\hat{\mathfrak{R}}_N(\mathcal{F}) = \sum_{j=1}^k \hat{\mathfrak{R}}_N(\mathcal{F}_j). \quad (9)$$

Theorem 3.1 (Generalization Error for Policy Distillation)

Assume that the loss function ℓ is Lipschitz continuous with Lipschitz constant L_ℓ with respect to its first argument, and bounded by C . Then, with probability at least $1 - \delta$, for all $\theta \in \Theta$:

$$\mathcal{L}(\pi_\theta) \leq \hat{\mathcal{L}}(\pi_\theta) + 2L_\ell \hat{\mathfrak{R}}_N(\mathcal{F}) + C \sqrt{\frac{\log(1/\delta)}{2N}},$$

where $\mathcal{L}(\pi_\theta) = \mathbb{E}[\ell(\pi_\theta, \pi^*)]$ is the expected loss of visuomotor policy π_θ to expert policy π_e and $\hat{\mathcal{L}}(\pi_\theta)$ is the empirical loss as defined in Eqn. (7). The Rademacher complexity $\hat{\mathfrak{R}}_N(\mathcal{F}) = \mathbb{E}[\hat{\mathfrak{R}}_N(\mathcal{F})]$.

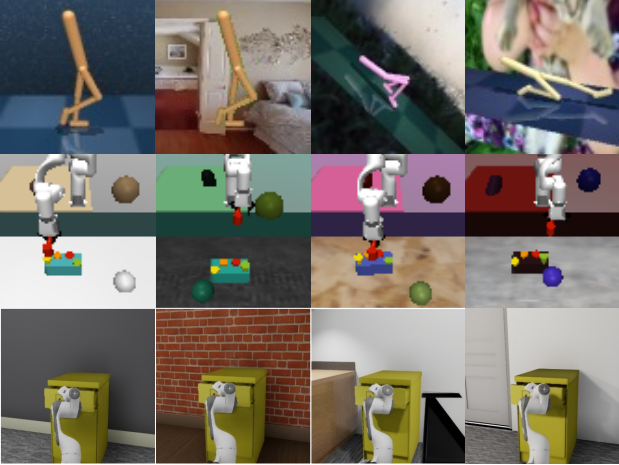


Figure 3. Observation examples from three benchmarks. Top row: DMC-GB (first: training, second: video hard setting, last two: distraction setting). Medium row: Enhanced Robot Manipulation Distraction Benchmark (first: training, last three: testing). Bottom row: Self-designed Drawer Opening Generalization Benchmark (first: training, second: different backgrounds, last two: different scenarios).

Proof is detailed in [23]. Obviously, the generalization error largely depends on the sample size. Although simply increasing N does not linearly reduce error, data augmentation—specifically *strong augmentation*—can effectively diversify data distribution and reduce Rademacher complexity. However, indiscriminate data augmentation across whole observations could distort crucial control information, leading to unpredictable increases in control prediction errors $\hat{\mathcal{L}}(\pi_\theta)$. Optimally, augmenting only control-irrelevant data while preserving essential control information can effectively reduce generalization errors by increasing the number of data samples while maintaining low prediction errors. Furthermore, direct guidance from expert policies simplifies training visuomotor policies by constraining the output space and reducing Rademacher complexity.

4. Experiments

To demonstrate the zero-shot generalization capabilities of EAGLE, we conducted experiments across three domains, as shown in Fig. 3:

Firstly, we evaluated EAGLE using the DMControl Generalization Benchmark (DMC-GB) [16], which tests an agent’s generalization ability from a simple to a complex environment. We employed three settings here: video-easy, video-hard, and distraction. In video-hard, the background features real-world videos, significantly different from the training environment. In distraction setting, the background image, foreground color, and camera view are varied in multiple difficulty level. Each method undergoes

500k training iterations, with evaluations based only on visual inputs.

Secondly, we introduced an enhanced Robot Manipulation Distraction Benchmark (RMDB), building on the original benchmark [2, 21] that includes four tasks: Push, Reach, Hammer, and Pegbox. We incorporated distraction objects in training, and varied colors/textures in five test environments. RMDB presents a greater challenge as it requires robots to develop a visuomotor policy robust to visual changes in all task-irrelevant areas (as shown in Fig. 3, where the pegbox changes to purple and brown). More detailed descriptions of RMDB can be found in Appendix 8.

Finally, we design a Drawer Opening Generalization Benchmark (DOGB) that utilizes the high-fidelity NVIDIA Isaac Sim for tasks involving the opening of a drawer against large-scale background and scenario variance. A task is considered successful if the drawer opens beyond 0.29 meters within 500 time steps. Compared to RMDB, DOGB demands more precise control over the 7-DoF robot arm and 2-DoF grasp, and copes with extensive background variations (up to 400 testing environments with the change of colors, patterns, and materials of the wallpaper and the carpet).

We compared EAGLE to the several SOTA algorithms [2, 16, 17, 27, 47, 49, 50, 53] in terms of generalization ability. Besides, we developed a strong baseline SAM+E that combined the large vision model SAM [26] with our privilege expert. A detailed description of our settings for SAM+E and its segmentation results on DMC-GB can be found in the Appendix 6.2.

4.1. Comparisons

Evaluation on DMC-GB. We conducted experiments on 7 tasks on DMC-GB following SOTA methods [2, 47] including Ball in cup, Cartpole swingup (denoted as Cartpole), Walker walk, Walker stand, Finger spin, Cheetah run and Finger turn easy (Denoted as Finger turn). Overall, EAGLE achieves a significant generalization performance improvement on video-hard settings, which is 17.4% higher than previous SOTA method SGQN.

We also notice that with advanced vision capabilities, SAM+E demonstrates notable generalization ability on certain tasks in the video-hard category, such as Finger Spin and Finger Turn. However, for other tasks like Walker Walk, performance in the video-hard setting declines by 56.6% compared to the video-easy setting. This decrease can be attributed to the Walker environment, where the moving robot may be misclassified as background due to predefined point prompts, leading to the erroneous deletion of task-irrelevant pixels for *strong augmentation*. This observation supports our intuition about applying data augmentation specifically to pixels that are irrelevant to the task. In contrast to SAM+E, our method, which incorpo-

Table 1. **DMC-GB Generalization Performance.** We report the episode returns over five random seeds. Δ represents the improvement of EAGLE over the second-best results. *Italicized numbers* indicate average results reported using one officially pre-released model. The best performance is highlighted in bold and the second-best is underlined.

Setting	Easy Task	DrQ	DrQ-v2	RAD	SODA	SVEA	TLDA	VAI	SAM+E	SGQN	EAGLE	Δ
Video easy	Ball in cup	380 \pm 188	401 \pm 67	363 \pm 158	<u>939 \pm 10</u>	928 \pm 43	892 \pm 68	909 \pm 44	<i>925</i>	889 \pm 87	973 \pm 9	+34
	Cartpole	459 \pm 81	267 \pm 26	473 \pm 54	742 \pm 73	772 \pm 46	671 \pm 57	729 \pm 19	<u>777</u>	770 \pm 56	861 \pm 6	+84
	Walker walk	747 \pm 21	196 \pm 52	608 \pm 92	771 \pm 66	839 \pm 29	873 \pm 34	871 \pm 42	<i>823</i>	<u>881 \pm 18</u>	929 \pm 17	+48
	Walker stand	926 \pm 30	487 \pm 83	879 \pm 64	905 \pm 7	947 \pm 11	<u>973 \pm 6</u>	948 \pm 12	<i>910</i>	950 \pm 10	978 \pm 12	+5
	Finger spin	599 \pm 62	491 \pm 35	516 \pm 113	783 \pm 51	737 \pm 93	744 \pm 18	932 \pm 2	<i>859</i>	<u>947 \pm 16</u>	934 \pm 7	-13
	Cheetah run	154 \pm 22	79 \pm 8	104 \pm 5	190 \pm 48	275 \pm 3	336 \pm 57	322 \pm 35	<u>444</u>	257 \pm 49	463 \pm 13	+19
	Finger turn	230 \pm 29	358 \pm 68	172 \pm 63	150 \pm 50	197 \pm 98	208 \pm 35	445 \pm 36	<u>645</u>	547 \pm 267	721 \pm 13	+76
	Average	499	326	445	640	671	671	703	769	749	837	+36(4.3%)
Video hard	Ball in cup	100 \pm 40	83 \pm 20	98 \pm 40	381 \pm 163	492 \pm 100	257 \pm 57	<i>524</i>	725	857 \pm 29	944 \pm 7	+87
	Cartpole	136 \pm 29	137 \pm 20	152 \pm 29	452 \pm 45	401 \pm 38	286 \pm 47	<i>378</i>	337	<u>537 \pm 33</u>	623 \pm 22	+86
	Walker walk	121 \pm 52	87 \pm 5	80 \pm 10	312 \pm 32	521 \pm 68	271 \pm 55	<u>823</u>	357	719 \pm 33	883 \pm 9	+60
	Walker stand	252 \pm 57	234 \pm 50	229 \pm 45	736 \pm 132	840 \pm 16	602 \pm 51	<u>931</u>	<i>612</i>	842 \pm 36	941 \pm 11	+10
	Finger spin	38 \pm 13	31 \pm 8	39 \pm 20	309 \pm 49	361 \pm 25	241 \pm 29	<i>752</i>	<u>772</u>	767 \pm 11	798 \pm 5	+26
	Cheetah run	74 \pm 24	34 \pm 6	98 \pm 19	155 \pm 16	157 \pm 14	90 \pm 27	<u>303</u>	<i>264</i>	238 \pm 37	435 \pm 2	+132
	Finger turn	236 \pm 47	159 \pm 8	155 \pm 9	155 \pm 16	237 \pm 15	104 \pm 18	<i>362</i>	<u>563</u>	461 \pm 64	565 \pm 10	+2
	Average	137	109	122	357	429	264	581	519	<u>631</u>	741	+110(17.4%)

rates a self-supervised, control-aware augmentation mask, consistently achieves high performance in both video-hard and video-easy settings. The convergence line of generalization performance on video-hard during training is shown in Fig. 9 in the Appendix. Clearly, our method achieves higher generalization performance compared to other methods within the same number of update iterations for the visuomotor policy

In addition, we evaluate EAGLE in more challenging distracting settings [43] with variations in foreground color, background video, and camera view in DMC-GB. As shown in Fig. 4, EAGLE consistently outperforms other strong baselines across all tasks. Particularly, in Cheetah Run, EAGLE achieves an average return of 301 under an intensity of 0.1, which is 68.9% higher than SAM+E (with a score of 195) and more than twice that of SGQN (with a score of 149). This improvement is attributable to the control-aware augmentation mask used by EAGLE, which augments all task-irrelevant regions, including some parts of the foreground, to enhance generalization ability. We also note that although SAM+E achieves high performance in some tasks on video-hard, it has difficulty generalizing against the foreground and camera views with purely visual segmentation.

Evaluation on RMDB. Table 2 shows the training and evaluation results of EAGLE and four other strong baselines on RMDB. Clearly, EAGLE achieves high performance in both the training and testing environments. For example, in the PegBox training task, EAGLE realizes a significant improvement—almost three times—in success rate compared to SGQN. Although SAM+E also achieves high performance in training, its generalization ability can be limited in some task. Specifically, it achieves 37% success rate in the testing environment for PegBox, which is 26% lower than that obtained by EAGLE. With the reliable guid-

ance of privileged Expert and a clear visual mask, SAM+E more easily learns a stable visuomotor control policy compared to other VRL methods. However, the visual mask is insufficient to handle visual variations from distracting objects, which are common in many robotic tasks. In contrast, the control-aware mask used by EAGLE augments the task-irrelevant regions in the observation space while preserving control-related information for decision-making.

In Fig. 5, we visualize the masks obtained by EAGLE and SAM for the tasks Hammer and Push. For Hammer, SAM identifies the entire robot arm, the hammer, the toy box, and two distracting balls as foreground, treating other regions as background. In contrast, EAGLE only captures parts of essential joints/links in the robot arm, the hammer, and the button in the toy box with the mask, augmenting other regions with *random conv*, as shown in the second and fourth pictures in the top row of Fig. 5. This selective preservation is enabled by the auxiliary losses in Eqn. (5), which ensures that only the most control-related areas are maintained for control prediction. It is important to note that EAGLE can capture all control-related regions, regardless of whether they are dynamic or static. For example, in Push task, the robot must push a green box towards a static red target throughout an episode, yet EAGLE still captures this for minimizing control prediction loss. Thus, with essential goal information carefully preserved, the training and testing performance of EAGLE are both superior compared to other baselines. More visualization results on RMDB and our detailed settings of SAM can be found in the appendix.

4.2. Ablation studies

We further study how each component of EAGLE contributes to its generalization and stability. In this subsec-

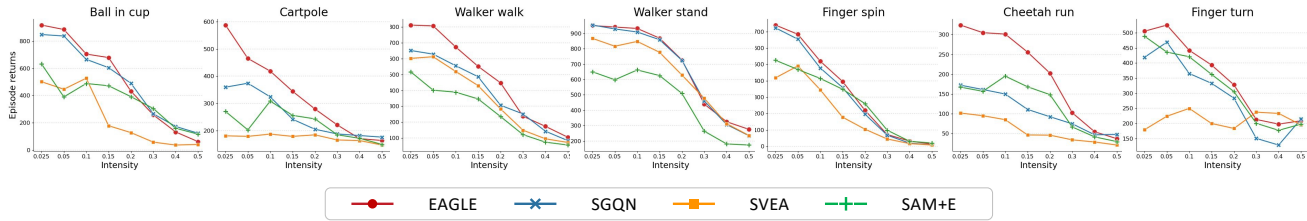


Figure 4. Generalization performance of all methods on DMC-GB distraction setting.

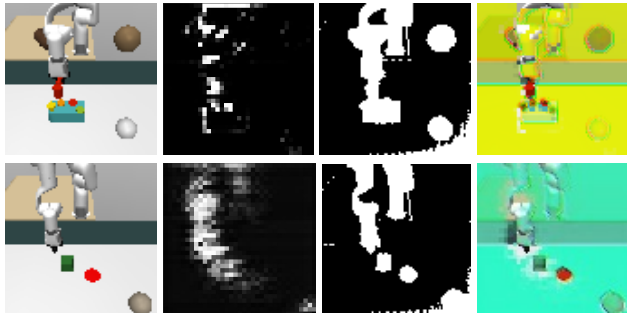


Figure 5. Illustration of the mask obtained by EAGLE and SAM on Hammer and Push. First column: original observations. Second column: EAGLE’s mask. Third column: SAM’s mask. Last column: control-aware augmented observations.

Table 2. Success rate on Robot Manipulation Generalization Performance. Test success rate denotes the average results across 5 different test environments.

Method	Hammer		Pegbox	
	Train	Test	Train	Test
SVEA	0.02	0.04 ± 0.02	0.42	0.03 ± 0.02
TLDA	0.22	0.02 ± 0.03	0.00	0.00 ± 0.01
VAI	0.00	0.01 ± 0.01	0.00	0.00 ± 0.00
SAM+E	0.46	0.06 ± 0.05	0.50	0.50 ± 0.15
SGQN	0.49	0.10 ± 0.12	0.21	0.05 ± 0.03
EAGLE	0.50	0.21 ± 0.06	0.58	0.54 ± 0.20
	Push		Reach	
	Train	Test	Train	Test
SVEA	0.30	0.30 ± 0.00	0.98	0.78 ± 0.23
TLDA	0.34	0.32 ± 0.04	0.98	0.96 ± 0.03
VAI	0.23	0.21 ± 0.02	0.80	0.36 ± 0.19
SAM+E	0.68	0.37 ± 0.07	1.00	0.99 ± 0.01
SGQN	0.38	0.37 ± 0.01	1.00	0.98 ± 0.03
EAGLE	0.72	0.50 ± 0.10	1.00	1.00 ± 0.00

tion, we first conduct ablation studies of the control-aware augmentation module and the privilege-guided distillation module on DMC-GB and DOGB. Then, we investigate the extent of improvement that the privilege Expert brings

to other state-of-the-art (SOTA) methods on challenging RMDB tasks for these VRL methods. Lastly, we perform ablations on the loss function in Eqn. (5) on DMC-GB.

Ablation on Module Structure: We conducted extensive ablation studies on EAGLE to evaluate the effectiveness of the control-aware data augmentation module and the privilege-guided distillation module. As shown in Tab. 3, we designed four ablation conditions for comparison: 1) **Q-only**: the vanilla DrQ-v2 algorithm with random shift augmentation. 2) **Q+Aug**: this method applies *random overlay* augmentation to **Q-only**. 3) **Q+Mask**: this method adds a control-aware attention mask to **Q+Aug**. It can be considered as EAGLE w/o. Expert module. 4) **E+Aug**: this method utilizes privilege-guided policy distillation and applies *random overlay* to the input image. It can be considered as EAGLE w/o. Mask module.

In Tab. 3, we find that applying strong augmentation directly to the DRL baseline (Q-only) can degrade policy performance, even in the training environment. For example, in the Walker walk task, Q+Aug achieved a training score of 435.6, which is 7% lower than Q-only. In contrast, as demonstrated by Q+Mask and E+Aug, both the control-aware attention mask and the privilege expert utilize overlay augmentation to enhance training and generalization performance on DMC-GB. Specifically, Q+Mask and E+Aug achieved average increases of 44% and 99% in training performance, respectively, and 239% and 323% in the video-easy environment.

It is worth noting that in most tasks under the video-hard setting, the control-aware augmentation module significantly improves generalization performance, whereas the privilege expert module reduces performance variability. For example, in Walker Walk, Q+Mask resulted in a 453% increase over Q-only, but with a high variance of 136. In contrast, E+Aug improved generalization with a much lower variance of 44. Therefore, by integrating the control-aware attention mask and privilege-guided distillation module, EAGLE achieves a remarkable improvement of 908% in Walker Walk. This underscores the joint effect of two modules in enhancing the efficient generalization of visuomotor policies.

We conducted ablation studies to validate our method on

Table 3. Ablation study of our control-aware attention module (denoted as Att.), privilege-guided distillation module (denoted as Exp.) and the random overlay augmentation (denoted as Aug.) on DMC-GB. We designed four ablation methods for comparison. 1) Q-only, 2) Q+Aug, 3) Q+Mask and 4) E+Aug.

Setting		Q.	Aug.	Att.	Exp.	Ball in cup	Walker walk	Walker stand	Finger spin	Finger turn	Cheetah run	Average
Train	Q-only	✓				678.1 ± 387	467.7 ± 120	872.7 ± 92.1	839.3 ± 51	454.2 ± 300	457.3 ± 293.8	628.3
	Q+Aug	✓	✓			766.8 ± 203(+13%)	435.6 ± 29(-7%)	473.2 ± 331(-46%)	658.4 ± 29(-22%)	246.8 ± 41(-45.7%)	227.6 ± 92(-50.2%)	468.0
	Q+Mask	✓	✓	✓		801.1 ± 120(+18%)	673.1 ± 185(+44%)	965.6 ± 7(+11%)	844.6 ± 22(0%)	679.2 ± 16(49%)	256.8 ± 12(-44%)	702.9
	E+Aug		✓	✓	✓	970.2 ± 2(+43%)	931.4 ± 34(+99%)	907.4 ± 25(+4%)	843.5 ± 23(+1%)	914.6 ± 55(+101.4%)	393.9 ± 11(-13.9%)	826.9
	EAGLE		✓	✓	✓	968.2 ± 8(+43%)	946.4 ± 5(+102%)	952.1 ± 15(+9%)	839.3 ± 8(+0%)	788.0 ± 47(+73%)	838.8 ± 15(+83%)	888.8
Video easy	Q-only	✓				401.3 ± 67	195.7 ± 52	487.0 ± 83	490.6 ± 35	258.3 ± 68	78.5 ± 8	318.6
	Q+Aug	✓	✓			722.9 ± 169.3(+80%)	369.7 ± 12(+89%)	478.6 ± 329.3(-2%)	586.5 ± 20(+20%)	212.9 ± 85(-18%)	212.6 ± 62(+171%)	430.60
	Q+Mask	✓	✓	✓		724.7 ± 107(+81%)	633.2 ± 174(+239%)	961.3 ± 2(+239%)	767.9 ± 19(+239%)	298.2 ± 18(16%)	296.4 ± 53(+278%)	613.0
	E+Aug		✓	✓	✓	954.8 ± 12(+138%)	828.1 ± 59(+323%)	886.2 ± 41(+82%)	741.0 ± 8(+51%)	577.8 ± 13(+124%)	325.4 ± 11(+314%)	718.9
	EAGLE		✓	✓	✓	973.4 ± 9(+143%)	929.3 ± 17(+375%)	978.5 ± 12(+101%)	934.1 ± 7(+70%)	721.3 ± 13(+179%)	463.2 ± 13(+490%)	833.3
Video hard	Q-only	✓				83.4 ± 20	87.4 ± 5	233.5 ± 50	30.7 ± 8	158.9 ± 8	34.1 ± 6	104.7
	Q+Aug	✓	✓			313.1 ± 108(+271%)	233.3 ± 34(+167%)	382.9 ± 245(+64%)	276.6 ± 15(+801%)	225.2 ± 62(+42%)	113.0 ± 10(+231%)	257.3
	Q+Mask	✓	✓	✓		459.5 ± 31(+451%)	483.4 ± 136(+453%)	910.4 ± 17(+290%)	724.9 ± 10(+2216%)	294.2 ± 31(+85%)	183.2 ± 11(+437%)	509.3
	E+Aug		✓	✓	✓	657.4 ± 28(+688%)	457.8 ± 44(+424%)	666.4 ± 13(+185%)	363.9 ± 9(+1085%)	394.5 ± 48(+149%)	104.9 ± 12(+208%)	440.5
	EAGLE		✓	✓	✓	944.0 ± 7(+1032%)	882.5 ± 75(+908%)	941.3 ± 11(+303%)	797.9 ± 5(+2499%)	565.3 ± 10(+256%)	435.1 ± 2(+1179%)	761.3

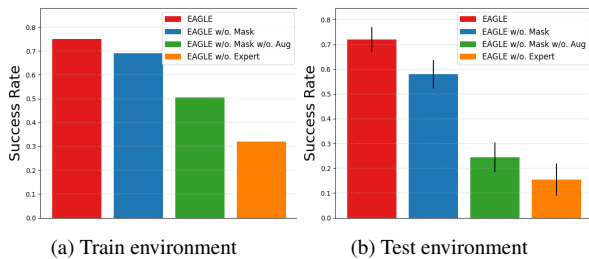


Figure 6. Ablation performance on DOGB.

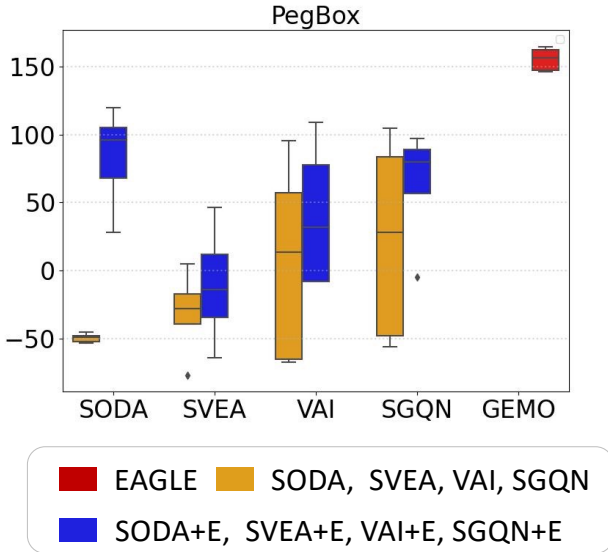


Figure 7. Improvements on baselines with privilege expert.

a long-horizontal drawer opening task in DOGB. As shown in Fig. 6, when facing unseen backgrounds, EAGLE consistently achieved an average success rate of 72% across large-scale testing environments. In contrast, EAGLE w/o. Expert showed significantly lower performance, with suc-

cess rates of 32% and 16% in the training and testing environments, respectively, demonstrating the importance of the privileged Expert in handling more challenging tasks. Additionally, while EAGLE w/o. Mask performed comparably to the EAGLE in the training environment, it exhibited poor generalization in the testing environment, highlighting the contribution of our attention mask for generalization.

Combine Expert module with other baselines. We investigated whether the Expert module could consistently enhance the generalization performance across other baselines besides SAM. We integrated the Expert with SODA, SVEA, VAI, and SGQN on RMDDB, considering the challenging Pegbox task for VRL methods on this benchmark. As shown in Fig. 7, the Expert module notably improved the generalization ability of other baselines. For example, SGQN+E achieved almost a two-times increase in the average returns, from 22 to 63, after incorporating the Expert module, along with a 44.6% reduction in variance. This demonstrates the importance of leveraging privileged information in the training environment when addressing challenging robotic tasks. Additionally, we observed that after integration with the Expert, EAGLE continued to outperform other methods, attributable to the control-aware augmentation module in EAGLE that selectively applies augmentation to task-irrelevant regions, thus consistently enhancing generalization performance during training.

Ablation on the loss function. In Eqn. 5, we formulate a self-supervised reconstruction task along with three auxiliary losses to derive a control-aware mask for augmentation. We conducted ablation studies of these three losses on DMC-GB. The convergence results for the video-hard settings of Walker walk and Walker stand are shown in Fig. 8, with additional results available in the appendix. Notably, the sparsity loss is crucial for generalization; otherwise, the generalization policy may collapse. Then, we can observe that the control prediction loss, \mathcal{L}_{ctl} , significantly enhances sample efficiency. For example, in Walker Stand, EAGLE rapidly converged to a generalizable visu-

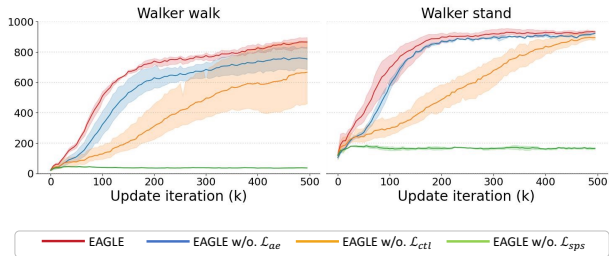


Figure 8. Ablation study of our control prediction loss and the auto-encoder loss in our augmentation module.

Table 4. Efficiency comparison of EAGLE vs. other methods regarding mask generation.

Method	EAGLE	VAI	SGQN	TLDA	SAM
time (ms) per image ↓	1.028	4.989	8.692	10.668	329.941

motor policy within 200k training iterations, whereas EAGLE without \mathcal{L}_{ctl} only reached similar performance levels at 500k update iterations and exhibited higher variance. This efficiency stems from \mathcal{L}_{ctl} 's ability to focus the model on the most critical regions for decision-making, given the constraints of the limited mask region. Additionally, the auto-encoder loss l_{ae} impacts tasks differently. In Walker walk, overlooking l_{ae} leads to high variance and unstable generalization performance. Conversely, in Walker stand, its influence on stability is minimal.

4.3. Efficiency comparison

Mask generating time efficiency. We evaluated the efficiency of EAGLE relative to four other methods by measuring the time required for mask generation in augmentation or consistency learning. Specifically, VAI [47] uses a reconstruction structure similar to EAGLE, but it generates masks through a decoder network using a predefined threshold. SGQN [2] produces sharp saliency maps by calculating policy gradients, which are then used in a consistency loss. TLDA [53] derives masks by computing the Lipschitz constant based on policy changes before and after image perturbation. SAM [26] generates masks based on given point prompts. Although these methods only compute masks during training, the inference time for masks can significantly affect training efficiency due to the large observation space. We computed the average mask inference time (in milliseconds) per image over 15,000 iterations. All evaluations were conducted on an Ubuntu 18.04 server equipped with an 8GB NVIDIA GTX 1180 graphics card and a 12-core AuthenticAMD CPU. As shown in Tab. 4, EAGLE demonstrates time efficiency in mask generation, contributing to the lightweight encoder in our implementation and the direct usage of the latent attention mask without decoding.

Training efficiency. We assessed the training efficiency

Table 5. Training Efficiency comparison of EAGLE vs. other SOTAs.

Method	Expert	EAGLE	SVEA	SODA	SGQN	SAM+E	TLDA
training time (h) ↓	0.9	8.3	9.0	8.0	16.3	22.8	61.3

of EAGLE in comparison with other SOTA methods, as detailed in Tab. 5. The average time efficiency across seven tasks in DMC-GB is provided. **Expert** denotes the privileged expert utilized in EAGLE. Notably, EAGLE demonstrates high training efficiency, characterized by both reduced training times and enhanced generalization performance. For example, while SGQN achieved well generalization performance in DMC-GB, it requires twice the training time of EAGLE. Despite requiring similar training times as SVEA and SODA, EAGLE achieves a remarkable average reward of 741 in the DMC-GB video-hard settings, which is 72.4% and 107.6% higher than that achieved by SVEA and SODA, respectively, as shown in Tab. 1.

5. Conclusion

In this paper, we address the generalization challenge of visuomotor policies in the face of visual changes. We propose an Efficient trAining framework for GeneraLizable visuomotor policies (EAGLE) designed to identify control-related regions and facilitate zero-shot generalization to unseen environments. EAGLE comprises two jointly optimized modules: a control-aware augmentation module and a privilege-guided policy distillation module. The former leverages a self-supervised reconstruction task with three auxiliary losses to learn a control-aware attention mask, which distinguishes task-irrelevant pixels and applies *strong augmentations* to minimize generalization gaps. The latter distills knowledge from a pretrained privileged expert into the visuomotor policies. We conduct extensive comparative and ablation studies across three challenging benchmarks to assess the efficacy of EAGLE. The experimental results well validate the effectiveness of our approach.

References

- [1] Andrea Banino, Caswell Barry, Benigno Uria, Charles Blundell, Timothy Lillicrap, Piotr Mirowski, Alexander Pritzel, Martin J Chadwick, Thomas Degris, Joseph Modayil, et al. Vector-based navigation using grid-like representations in artificial agents. *Nature*, 557(7705):429–433, 2018. 1
- [2] David Bertoin, Adil Zouitine, Mehdi Zouitine, and Emmanuel Rachelson. Look where you look! saliency-guided q-networks for visual rl tasks. *Advances in neural information processing systems*, 2022. 1, 2, 5, 9
- [3] Dian Chen, Brady Zhou, Vladlen Koltun, and Philipp Krähenbühl. Learning by cheating. In *Conference on Robot Learning*, pages 66–75. PMLR, 2020. 2, 4
- [4] Xi Chen, Ali Ghadirzadeh, Mårten Björkman, and Patric Jensfelt. Adversarial feature training for generalizable

- robotic visuomotor control. In *2020 IEEE International Conference on Robotics and Automation (ICRA)*, pages 1142–1148. IEEE, 2020. 1
- [5] Hyesong Choi, Hunsang Lee, Seongwon Jeong, and Dongbo Min. Environment agnostic representation for visual reinforcement learning. In *Proceedings of the IEEE/CVF International Conference on Computer Vision*, pages 263–273, 2023. 1
- [6] Karl Cobbe, Oleg Klimov, Chris Hesse, Taehoon Kim, and John Schulman. Quantifying generalization in reinforcement learning. In *International Conference on Machine Learning*, pages 1282–1289. PMLR, 2019. 2
- [7] Karl Cobbe, Chris Hesse, Jacob Hilton, and John Schulman. Leveraging procedural generation to benchmark reinforcement learning. In *International conference on machine learning*, pages 2048–2056. PMLR, 2020. 2
- [8] Wojciech M Czarnecki, Razvan Pascanu, Simon Osindero, Siddhant Jayakumar, Grzegorz Swirszcz, and Max Jaderberg. Distilling policy distillation. In *The 22nd international conference on artificial intelligence and statistics*, pages 1331–1340. PMLR, 2019. 2
- [9] Alexey Dosovitskiy, German Ros, Felipe Codevilla, Antonio Lopez, and Vladlen Koltun. Carla: An open urban driving simulator. In *Conference on robot learning*, pages 1–16. PMLR, 2017. 2
- [10] Jiameng Fan and Wenchao Li. Dribo: Robust deep reinforcement learning via multi-view information bottleneck. In *International Conference on Machine Learning*, pages 6074–6102. PMLR, 2022. 2
- [11] Linxi Fan, Guanzhi Wang, De-An Huang, Zhiding Yu, Li Fei-Fei, Yuke Zhu, and Animashree Anandkumar. Secant: Self-expert cloning for zero-shot generalization of visual policies. In *International Conference on Machine Learning*, pages 3088–3099. PMLR, 2021. 1, 2, 4
- [12] Xiang Fu, Ge Yang, Pulkit Agrawal, and Tommi Jaakkola. Learning task informed abstractions. In *International Conference on Machine Learning*, pages 3480–3491. PMLR, 2021. 1
- [13] Alexandre Galashov, Josh S Merel, and Nicolas Heess. Data augmentation for efficient learning from parametric experts. *Advances in Neural Information Processing Systems*, 35: 31484–31496, 2022. 2
- [14] Tuomas Haarnoja, Aurick Zhou, Pieter Abbeel, and Sergey Levine. Soft actor-critic: Off-policy maximum entropy deep reinforcement learning with a stochastic actor. In *International conference on machine learning*, pages 1861–1870. PMLR, 2018. 2
- [15] Siddhant Halder, Vaibhav Mathur, Denis Yarats, and Lerrel Pinto. Watch and match: Supercharging imitation with regularized optimal transport. In *Conference on Robot Learning*, pages 32–43. PMLR, 2023. 4, 1
- [16] Nicklas Hansen and Xiaolong Wang. Generalization in reinforcement learning by soft data augmentation. In *2021 IEEE International Conference on Robotics and Automation (ICRA)*, pages 13611–13617. IEEE, 2021. 1, 2, 4, 5
- [17] Nicklas Hansen, Hao Su, and Xiaolong Wang. Stabilizing deep q-learning with convnets and vision transformers under data augmentation. *Advances in neural information processing systems*, 34:3680–3693, 2021. 1, 2, 5
- [18] Alex Hernández-García and Peter König. Data augmentation instead of explicit regularization. *arXiv preprint arXiv:1806.03852*, 2018. 4
- [19] Maximilian Igl, Kamil Ciosek, Yingzhen Li, Sebastian Tschitschek, Cheng Zhang, Sam Devlin, and Katja Hofmann. Generalization in reinforcement learning with selective noise injection and information bottleneck. *Advances in neural information processing systems*, 32, 2019. 2
- [20] Maximilian Igl, Gregory Farquhar, Jelena Luketina, Wendelin Boehmer, and Shimon Whiteson. The impact of non-stationarity on generalisation in deep reinforcement learning. *arXiv preprint arXiv:2006.05826*, 2020. 2
- [21] Rishabh Jangir, Nicklas Hansen, Sambaran Ghosal, Mohit Jain, and Xiaolong Wang. Look closer: Bridging egocentric and third-person views with transformers for robotic manipulation. *IEEE Robotics and Automation Letters*, 7(2):3046–3053, 2022. 2, 5
- [22] Niels Justesen, Ruben Rodriguez Torrado, Philip Bontrager, Ahmed Khalifa, Julian Togelius, and Sebastian Risi. Illuminating generalization in deep reinforcement learning through procedural level generation. *NeurIPS Workshop on Deep Reinforcement Learning Workshop*, 2018. 2
- [23] Sham M Kakade, Karthik Sridharan, and Ambuj Tewari. On the complexity of linear prediction: Risk bounds, margin bounds, and regularization. *Advances in neural information processing systems*, 21, 2008. 5
- [24] Dmitry Kalashnikov, Alex Irpan, Peter Pastor, Julian Ibarz, Alexander Herzog, Eric Jang, Deirdre Quillen, Ethan Holly, Mrinal Kalakrishnan, Vincent Vanhoucke, et al. Scalable deep reinforcement learning for vision-based robotic manipulation. In *Conference on Robot Learning*, pages 651–673. PMLR, 2018. 1
- [25] Mete Kemertas and Tristan Aumentado-Armstrong. Towards robust bisimulation metric learning. *Advances in Neural Information Processing Systems*, 34:4764–4777, 2021. 2
- [26] Alexander Kirillov, Eric Mintun, Nikhila Ravi, Hanzi Mao, Chloe Rolland, Laura Gustafson, Tete Xiao, Spencer Whitehead, Alexander C Berg, Wan-Yen Lo, et al. Segment anything. *arXiv preprint arXiv:2304.02643*, 2023. 1, 2, 4, 5, 9
- [27] Misha Laskin, Kimin Lee, Adam Stooke, Lerrel Pinto, Pieter Abbeel, and Aravind Srinivas. Reinforcement learning with augmented data. *Advances in neural information processing systems*, 33:19884–19895, 2020. 5
- [28] Joonho Lee, Jemin Hwangbo, Lorenz Wellhausen, Vladlen Koltun, and Marco Hutter. Learning quadrupedal locomotion over challenging terrain. *Science robotics*, 5(47):eabc5986, 2020. 2, 4
- [29] Kimin Lee, Kibok Lee, Jinwoo Shin, and Honglak Lee. Network randomization: A simple technique for generalization in deep reinforcement learning. *International Conference on Learning Representations*, 2019. 1, 4
- [30] Lu Li, Jiafei Lyu, Guozheng Ma, Zilin Wang, Zhenjie Yang, Xiu Li, and Zhiheng Li. Normalization enhances generalization in visual reinforcement learning. In *Proceedings of the*

- 23rd International Conference on Autonomous Agents and Multiagent Systems, pages 1137–1146, 2024. 2
- [31] Jiashun Liu, HAO Jianye, Yi Ma, and Shuyin Xia. Unlock the cognitive generalization of deep reinforcement learning via granular ball representation. In *International Conference on Machine Learning*. PMLR, 2024. 2
- [32] Qiyuan Liu, Qi Zhou, Rui Yang, and Jie Wang. Robust representation learning by clustering with bisimulation metrics for visual reinforcement learning with distractions. In *Proceedings of the AAAI Conference on Artificial Intelligence*, pages 8843–8851, 2023. 2
- [33] Marlos C Machado, Marc G Bellemare, Erik Talvitie, Joel Veness, Matthew Hausknecht, and Michael Bowling. Revisiting the arcade learning environment: Evaluation protocols and open problems for general agents. *Journal of Artificial Intelligence Research*, 61:523–562, 2018. 2
- [34] Viktor Makoviychuk, Lukasz Wawrzyniak, Yunrong Guo, Michelle Lu, Kier Storey, Miles Macklin, David Hoeller, Nikita Rudin, Arthur Allshire, Ankur Handa, et al. Isaac gym: High performance gpu based physics simulation for robot learning. In *Thirty-fifth Conference on Neural Information Processing Systems Datasets and Benchmarks Track*, 2021. 2
- [35] Charles Packer, Katelyn Gao, Jernej Kos, Philipp Krähenbühl, Vladlen Koltun, and Dawn Song. Assessing generalization in deep reinforcement learning. *arXiv preprint arXiv:1810.12282*, 2018. 2
- [36] Lerrel Pinto, Marcin Andrychowicz, Peter Welinder, Wojciech Zaremba, and Pieter Abbeel. Asymmetric actor critic for image-based robot learning. *arXiv preprint arXiv:1710.06542*, 2017. 2
- [37] Roberta Raileanu and Tim Rocktäschel. Ride: Rewarding impact-driven exploration for procedurally-generated environments. *International Conference on Learning Representations*, 2020. 2
- [38] Aravind Rajeswaran, Kendall Lowrey, Emanuel V Todorov, and Sham M Kakade. Towards generalization and simplicity in continuous control. *Advances in Neural Information Processing Systems*, 30, 2017. 2
- [39] Nikhila Ravi, Valentin Gabeur, Yuan-Ting Hu, Ronghang Hu, Chaitanya Ryali, Tengyu Ma, Haitham Khedr, Roman Rädle, Chloe Rolland, Laura Gustafson, et al. Sam 2: Segment anything in images and videos. *arXiv preprint arXiv:2408.00714*, 2024. 2, 4
- [40] Sasha Salter, Dushyant Rao, Markus Wulfmeier, Raia Hadsell, and Ingmar Posner. Attention-privileged reinforcement learning. In *Conference on Robot Learning*, pages 394–408. PMLR, 2021. 2
- [41] Max Schwarzer, Ankesh Anand, Rishab Goel, R Devon Hjelm, Aaron Courville, and Philip Bachman. Data-efficient reinforcement learning with self-predictive representations. *International Conference on Learning Representations*, 2020. 1
- [42] Nitish Srivastava, Geoffrey Hinton, Alex Krizhevsky, Ilya Sutskever, and Ruslan Salakhutdinov. Dropout: a simple way to prevent neural networks from overfitting. *The journal of machine learning research*, 15(1):1929–1958, 2014. 2
- [43] Austin Stone, Oscar Ramirez, Kurt Konolige, and Rico Jonschkowski. The distracting control suite—a challenging benchmark for reinforcement learning from pixels. *arXiv preprint arXiv:2101.02722*, 2021. 6
- [44] Ashish Vaswani, Noam Shazeer, Niki Parmar, Jakob Uszkoreit, Llion Jones, Aidan N Gomez, Łukasz Kaiser, and Illia Polosukhin. Attention is all you need. *Advances in neural information processing systems*, 30, 2017. 3
- [45] Che Wang, Xufang Luo, Keith Ross, and Dongsheng Li. Vrl3: A data-driven framework for visual deep reinforcement learning. In *Conference on Neural Information Processing Systems*, 2022. 4, 1
- [46] Huan Wang, Stephan Zheng, Caiming Xiong, and Richard Socher. On the generalization gap in reparameterizable reinforcement learning. In *International Conference on Machine Learning*, pages 6648–6658. PMLR, 2019. 2
- [47] Xudong Wang, Long Lian, and Stella X Yu. Unsupervised visual attention and invariance for reinforcement learning. In *Proceedings of the IEEE/CVF Conference on Computer Vision and Pattern Recognition*, pages 6677–6687, 2021. 1, 2, 3, 5, 9
- [48] Sizhe Yang, Yanjie Ze, and Huazhe Xu. Movie: Visual model-based policy adaptation for view generalization. *Advances in Neural Information Processing Systems*, 36, 2024. 2
- [49] Denis Yarats, Rob Fergus, Alessandro Lazaric, and Lerrel Pinto. Mastering visual continuous control: Improved data-augmented reinforcement learning. In *Deep RL Workshop NeurIPS 2021*, 2021. 1, 4, 5
- [50] Denis Yarats, Ilya Kostrikov, and Rob Fergus. Image augmentation is all you need: Regularizing deep reinforcement learning from pixels. In *International Conference on Learning Representations*, 2021. 1, 2, 5
- [51] Denis Yarats, Amy Zhang, Ilya Kostrikov, Brandon Amos, Joelle Pineau, and Rob Fergus. Improving sample efficiency in model-free reinforcement learning from images. In *Proceedings of the AAAI Conference on Artificial Intelligence*, pages 10674–10681, 2021. 2
- [52] Wenhao Yu, Deepali Jain, Alejandro Escontrela, Atil Iscen, Peng Xu, Erwin Coumans, Sehoon Ha, Jie Tan, and Tingnan Zhang. Visual-locomotion: Learning to walk on complex terrains with vision. In *5th Annual Conference on Robot Learning*, 2021. 1
- [53] Z Yuan, G Ma, Y Mu, B Xia, B Yuan, X Wang, P Luo, and H Xu. Don’t touch what matters: Task-aware lipschitz data augmentation for visual reinforcement learning. In *Proceedings of the Thirty-First International Joint Conference on Artificial Intelligence, Vienna, 23-29 July 2022*. International Joint Conferences on Artificial Intelligence., 2022. 2, 5, 9
- [54] Zhecheng Yuan, Zhengrong Xue, Bo Yuan, Xueqian Wang, Yi Wu, Yang Gao, and Huazhe Xu. Pre-trained image encoder for generalizable visual reinforcement learning. In *Advances in Neural Information Processing Systems*, 2022. 2
- [55] Zhecheng Yuan, Zhengrong Xue, Bo Yuan, Xueqian Wang, Yi Wu, Yang Gao, and Huazhe Xu. Pre-trained image encoder for generalizable visual reinforcement learning. In *Advances in Neural Information Processing Systems*, 2022. 4, 1

- [56] Amy Zhang, Nicolas Ballas, and Joelle Pineau. A dissection of overfitting and generalization in continuous reinforcement learning. *arXiv preprint arXiv:1806.07937*, 2018. [2](#)
- [57] Amy Zhang, Rowan McAllister, Roberto Calandra, Yarín Gal, and Sergey Levine. Learning invariant representations for reinforcement learning without reconstruction. *arXiv preprint arXiv:2006.10742*, 2020. [2](#)
- [58] Chiyuan Zhang, Oriol Vinyals, Remi Munos, and Samy Bengio. A study on overfitting in deep reinforcement learning. *arXiv preprint arXiv:1804.06893*, 2018. [2](#)
- [59] Tony Z Zhao, Vikash Kumar, Sergey Levine, and Chelsea Finn. Learning fine-grained bimanual manipulation with low-cost hardware. *arXiv preprint arXiv:2304.13705*, 2023. [3](#), [4](#)
- [60] Brady Zhou, Nimit Kalra, and Philipp Krähenbühl. Domain adaptation through task distillation. In *Computer Vision—ECCV 2020: 16th European Conference, Glasgow, UK, August 23–28, 2020, Proceedings, Part XXVI 16*, pages 664–680. Springer, 2020. [2](#)

Efficient Training of Generalizable Visuomotor Policies via Control-Aware Augmentation

Supplementary Material

6. Implementation Details

In this section, we first provide the implementation details for EAGLE, and then we provide the implementation details for a strong baseline SAM+E we utilized in our experiments.

6.1. Implementations of EAGLE

Algorithm details. We present the pseudocode of EAGLE in Algorithm 1. We first train the privileged expert given only the state information (i.e., the state s) using DrQv2 [49] (from line 5 to line 12). Note that any other standard RL algorithm can be applied here to replace DrQv2. In the second part of EAGLE (from line 13 to line 24), we train the control-aware data augmentation module and privilege-guided policy distillation module **simultaneously**. For the former module, we build our implementation on top of the convolutional block attention module (CBAM) which consists of a channel attention block and a spatial attention block. The channel attention block comprises an averaging operation module (an average-pooling function followed by two MLP layers) and a maxing operation module (a max-pooling function followed by two MLP layers). A sigmoid activation function is applied on the end to produce a channel mask. The spatial attention block comprises a channel pool function (to extract the maximum and average features across channels), convolutional layers (with a kernel size of 7, stride of 1, and padding of 3), and a batchnorm layer sequentially. More detailed network structures and parameter settings can be found in our open-source code.

Hyperparameter settings. In practice, we build our implementation on top of DrQv2 [49] due to its broad adoption in continuous control tasks [15, 45, 55] as well as a clean and efficient codebase. Therefore, EAGLE follows the hyperparameter settings from DrQ-v2, as listed in Tab. 6. Specifically, EAGLE introduces only one new hyperparameter λ to control the sparsity of the attention mask. After conducting ablation studies on the sparsity loss in Supplementary 7, we set λ to 0.001 for DMC-GB/DOGB and 0.01 for RMDB. For data augmentation methods, we use random overlay with Places365 for DMC-GB/DOGB and random conv for RMDB.

6.2. Implementations of SAM+E

SAM [26] is one of the most popular state-of-the-art (SOTA) large vision models that is capable of getting the segmentation results automatically with proper point prompts over various domains. Therefore, we use SAM

Algorithm 1 EAGLE

```
1:  $\pi_e, Q_1, Q_2$ : randomly initialized policy network and
   two value network for privileged expert
2:  $f_e(\cdot), f_d(\cdot), f_a(\cdot), f_{ctl}(\cdot, \cdot), :$  : randomly initialized en-
   coder, decoder, attention network and control predic-
   tion network in control-aware augmentation module
3:  $\pi$ : random initialized student policy network
4: replay buffer  $\mathcal{D}$ , mini-batch size  $b$ 
5: for Each interaction timestep  $i$  do
6:   Rollout  $\pi_e$  for one timestep and add  $(s_i, a_i, r_i)$  to
   dataset  $\mathcal{D} \leftarrow \mathcal{D} \cup (s_i, a_i, r_i)$ 
7:   if  $|\mathcal{D}| > b$  then
8:     Sample experiences  $(\mathbf{s}, \mathbf{a}, \mathbf{r}) \sim \mathcal{D}$ 
9:     Update  $\pi_e$ 
10:    Update  $Q_1, Q_2$ 
11:   end if
12: end for
13: Empty  $\mathcal{D} = \emptyset$ 
14: for Each interaction timestep  $t$  do
15:   Choose  $\pi_{roll}$  from  $\pi_e$  or  $\pi$ 
16:   Rollout  $\pi_{roll}$  for one timestep and add  $(o_t, s_t)$  to
   dataset  $\mathcal{D} \leftarrow \mathcal{D} \cup (o_t, s_t)$ 
17:   if  $|\mathcal{D}| > b$  then
18:     Sample experiences  $(\mathbf{o}, \mathbf{s}, \mathbf{o}') \sim \mathcal{D}$ 
19:     Update control-aware data augmentation mod-
   ule according to Equation 5
20:     Obtain control-aware augmented observation
    $\mathbf{o}_{aug}$  according to Equation 6
21:     Update  $\pi$  according to Equation 7
22:   end if
23: end for
```

to construct a strong baseline SAM+E. Considering the mask inference time, we use the ViT-B SAM model checkpoint. To get proper background prompts, we first upload an example image on Segment-Anything website and randomly sample points until we get a clear segmentation result. Then, we use an Image Position Coordinate Tool to get these prompts' positions. After configuring the point prompts, we check the segmentation results again with Weights&Biases.

The prompts we used in DMC-GB are (2, 80), (2, 57), (3, 7). The corresponding segmentation results we got with SAM are shown in Fig. 11. The prompts we used in RMDB are (2, 5), (2, 24), (2, 37), (2, 67). The corresponding segmentation results are shown in Fig. 12.

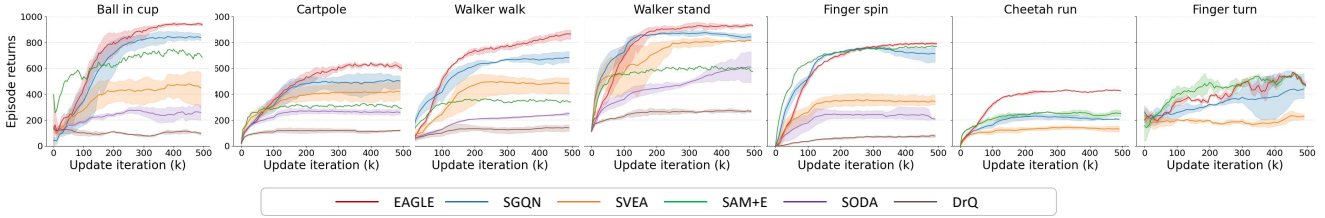


Figure 9. Generalization performance of all methods on DMC-GB video-hard.

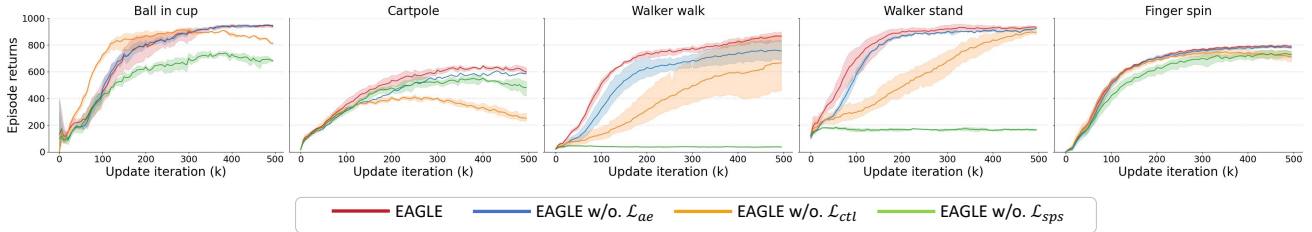


Figure 10. Ablation study on augmentation loss under DMC-GB video-hard.

Table 6. EAGLE Hyperparameters.

Hyperparameter	Value
Learning rate for all net	1e-4
Target update rate	0.01
Optimizer	Adam
Batch size	256
Discount factor	0.99
n-step	1 for Walker walk & Walker stand, 3 for others
Update interval	2
Replay buffer size	500k
Observation	84 × 84 for DMC-GB/RMDB, 128 × 128 for DOGB
Learning rate for all net	1e-4
Optimizer	Adam
Batch size	256
Frame stack	3 for DMC-GB, 1 for RMDB/DOGB
Update interval	2
Replay buffer size	500k for DMC-GB/RMDB, 100k for DOGB
λ	0.001 for DMC-GB, 0.01 for RMDB/DOGB
β	0.5
α in <i>random overlay</i>	linear schedule from 0.4 to 0.9

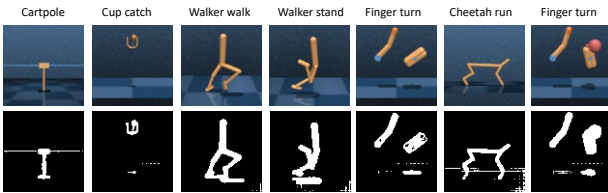


Figure 11. Segmentation results in DMC-GB with SAM.

7. Additional results on DMC-GB

In this section, we first provide more ablation results on DMC-GB. Then we provide more visualization results with EAGLE in DMC-GB.

7.1. Ablation study on the loss function

The original manuscript presented ablation results on the loss function for the Walker-walk and Walker-stand tasks.

In this section, we extend the ablation analysis to five tasks in DMC-GB, focusing on the loss terms \mathcal{L}_{rec} , \mathcal{L}_{ctl} , and \mathcal{L}_{sps} in Equ. 5.

Impact of \mathcal{L}_{ctl} . Apparently, the control prediction loss \mathcal{L}_{ctl} (represented by the orange line in Fig. 10) is crucial for the stability performance of EAGLE. Absence of \mathcal{L}_{ctl} may result in significant variance in policy generalization performance (as observed in Walker walk and Walker stand tasks) or lead to a performance decline during training (as shown in Ball in cup, Cartpole, and Finger spin tasks). This is due to the sparsity constraint applied in our method. This constraint may cause the augmentation module to distribute low values evenly across the entire dynamic foreground in EAGLE w/o. \mathcal{L}_{ctl} . Consequently, with a linear growing schedule in *random overlay*, some control-related parts (e.g., the tip of the cartpole) may be disrupted by the augmentation process, thus influencing the overall stability and performance of the model.

Impact of \mathcal{L}_{sps} . The sparsity loss \mathcal{L}_{sps} (represented by the green line in Fig. 10) is also crucial for generalization performance. In the absence of \mathcal{L}_{sps} , the model’s generalization ability may converge to a lower level or even experience policy degradation. This occurs because, in the absence of the sparsity constraint, the generated mask may focus on a control-irrelevant background or even the entire observation space (in the Walker environment). Without fully utilizing the augmentation technique, this, in turn, leads to an apparent performance decline in video-hard settings.

Impact of \mathcal{L}_{ae} . The effect of \mathcal{L}_{ae} (represented by the blue line in Fig. 10) is different across five tasks. Overall, by adding the auto-encoder loss, we could learn a stable and generalizable policy in various tasks.

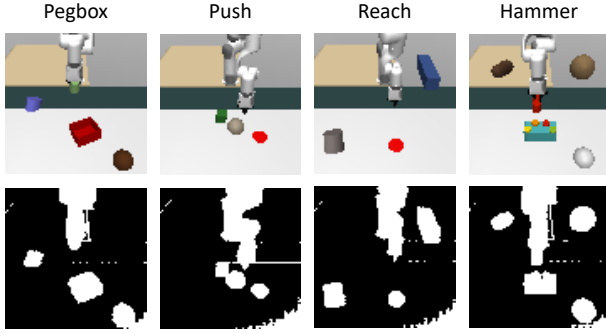


Figure 12. Segmentation results in RMDB with SAM.

7.2. Visualization of EAGLE on DMC-GB

In Fig. 13, we visualize the original observation o , the vanilla augmented observation $aug(o)$ with *random overlay* ($\alpha=0.8$), the control-aware mask m and the control-aware augmented observation o_{aug} . We clearly observed that, with our control-aware mask, EAGLE augments only the control-irrelevant regions while preserving the control-related parts. For example, when the walker is standing (in Walker stand), we preserve the some region of the "leg" and "head" of the robot. While the walker is walking (in Walker walk), we mainly concentrate on the "leg" and the "upper-body". With this control-aware augmentation module, we preserve the most control-related features for decision-making while augmenting other areas to enhance generalization.

8. Additional results on RMDB

8.1. Detail description of RMDB

Compared with the original Robot Manipulation benchmark, we made the following modifications in RMDB:

- For each task, we introduced 1-3 distractors on the front desk and/or background floor. The color of these distractors varies in each testing environment but remains consistent during training. We selected this configuration to assess the policy's generalization ability when facing visual appearance changes of these distractors.
- We revised the reward function in the Push task. The original function only considered control magnitude and the distance between the object and its target. We introduced an additional reward term to incentivize the robot arm to approach the object, facilitating learning.

Despite the aforementioned modifications, we follow the original Robot Manipulation benchmark to validate the policy across five testing environments, each with different visual changes to the front desk, background wall, and operating objects. The training environment examples can be found in Fig. 12. The testing environment examples can be found in Fig. 3.

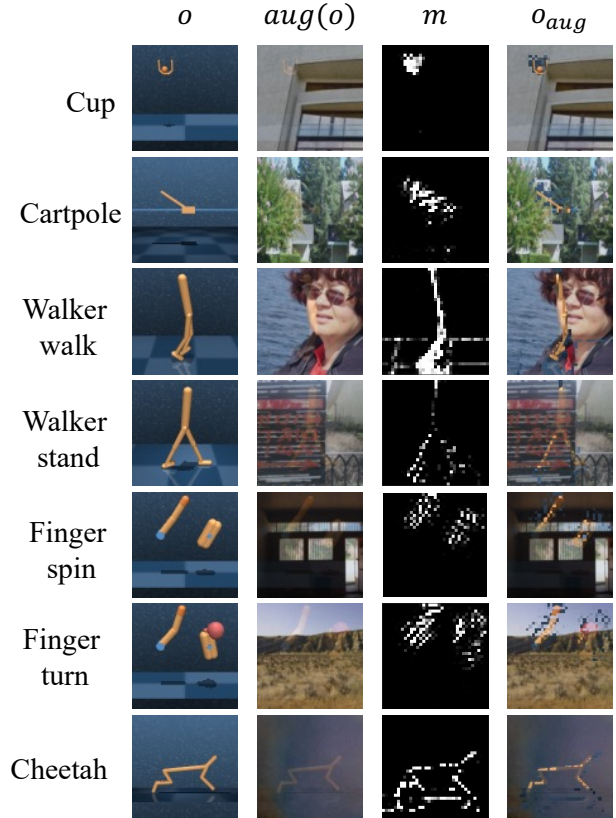


Figure 13. Visualization results of EAGLE in DMC-GB.

8.2. Visualization of EAGLE on RMDB

In Fig. 14, we demonstrate the original observation o , the vanilla augmented observation $aug(o)$ with *random conv*, the control-aware mask m and the control-aware augmented observation o_{aug} in RMDB. More detailed analysis and the comparison with the mask obtained by SAM can be found in Section. 4.1 in the manuscript.

9. Real world experiments

To validate EAGLE in real-world scenarios, we select a typical robot manipulation task of picking bread and placing it on a plate. We collect 200 trajectories using an expert policy and perform only offline distillation for safety considerations. As shown in Fig. 15, the student visuomotor policy receives inputs from three cameras (top: cropped to 720×720 ; left and right: cropped to 480×480) and the joint positions of the Franka Arm. The output action is a continuous vector consisting of seven joint positions and one gripper value. All image inputs are resized to 256×256 . The batch size is set to 16, and other parameters are the same as DOGB in Tab. 6. We use ACT [59] with ResNet50 as the backbone, and combine it with our control-aware augmen-

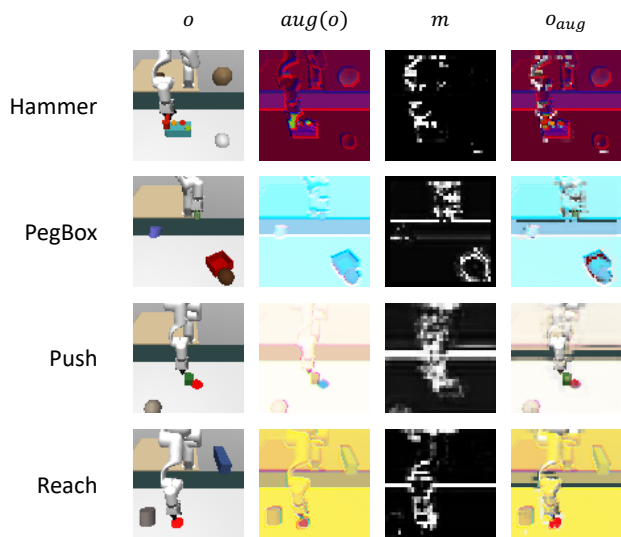


Figure 14. Visualization results of EAGLE in RMDB.

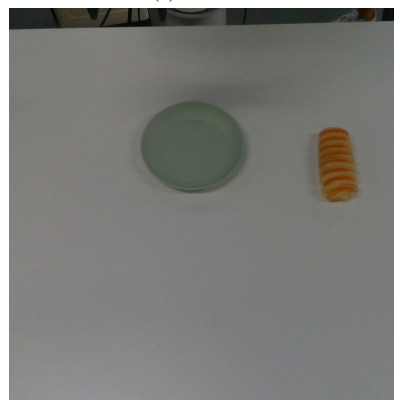
Method	Training	Testing (Change Background)	Testing (Add Distractors)
EAGLE	0.85	0.75	0.60
ACT [59]	0.80	0.00	0.00

Table 7. Real-world Experiments.

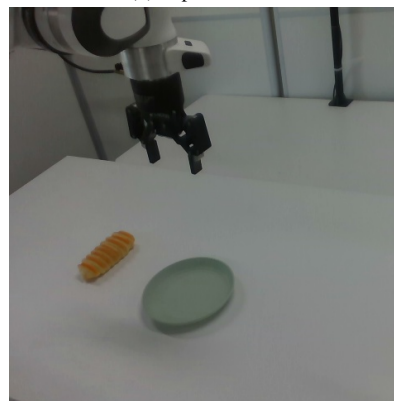
tation module and Random Conv techniques. We compare the generalization performance of EAGLE and ACT by averaging results over 20 trials with varying bread positions. As shown in Tab. 7, EAGLE significantly improves generalization when facing with changing backgrounds and added distractors, whereas the baseline ACT lacks such generalization without proper data augmentation.



(a) Left view



(b) Topdown view



(c) right view

Figure 15. Three camera views used in EAGLE.